PAPER

Check for updates

A benzothiazole-based new fluorogenic chemosensor for the detection of CN⁻ and its real-time application in environmental water samples and living cells†

Dhanapal Jothi, [iD] [a] Sathishkumar Munusamy,[b] Selin Manoj kumar,[a] Saravanan Enbanathan [iD] [a] and Sathiyanarayanan Kulathu Iyer [iD] *[a]

Since the cyanide ion is used in a wide range of industries and is harmful to both human health and the environment, a number of research efforts are dedicated to creating fluorescence sensors for the detection of cyanide (CN⁻). Herein, for the fluorescence detection of CN⁻, a new highly selective and sensitive sensor 2-(3-(benzo[*d*]thiazol-2-yl)-4-hydroxybenzylidene)-1*H*-indene-1,3(2*H*)-dione (**BID**) was created by conjugating a benzothiazole moiety with 1*H*-indene-1,3(2*H*)-dione. The donor and acceptor components of this hybrid receptor were covalently connected through a double bond. The nucleophilic addition of a cyanide anion to the **BID** inhibits the intramolecular charge transfer (ICT) transition, resulting in spectral and colour alterations in the receptor. When the solvent polarity was increased from *n*-hexane to methanol, this molecule exhibited a bathochromic shift in the emission wavelength (610 to 632 nm), suggesting the presence of a solvatochromic action. The sensor **BID** has shown strong specificity towards CN⁻ by interrupting its internal charge transfer (ICT), resulting in a significant change in the UV-vis spectrum and a notable blue shift in the fluorescence emission spectrum. The cyanide anion (CN⁻) is responsible for the optical alterations observed by **BID**, as opposed to the other anions examined. The detection limit was 5.97 nM, significantly less than the WHO's permitted amount of CN⁻ in drinking water. The experimental findings indicate that **BID**'s fluorescence response to CN⁻ is pH insensitive throughout a wide pH range of 6.0 to 12.0. The interaction mechanism between the **BID** and CN⁻ ions has been studied by HRMS, ¹H-NMR titration experiments, FT-IR, and DFT, which confirmed the nucleophilic addition of CN⁻ on vinylidene and subsequent disturbance of ICT. Additionally, we demonstrated the real-time detection application of CN⁻ in environmental water samples and live-cell imaging.

Introduction

Ions have a variety of important functions in chemical and biological processes.[1–9] Among them, many anions are naturally occurring, and they have significant roles in essential disciplines, including life science, chemistry, medicine, catalysis, and the environment.[10–14] To this end, for the past few years, anion recognition has become an area of growing concern in the field of environmental and biological sciences. Many types of anions are considered to be extremely dangerous, but one in particular, cyanide (CN⁻), has always been of interest all over the world because of its potency and universal presence in many processes such as manufacturing of plastic and fiber products, tanning, metallurgy, the petrochemical industry, herbicide production, chelators in water treatment, and silver or gold extraction. Despite its overwhelming application in various fields, CN⁻ is still harmful to humans even at a dosage of only 0.5 mg per kilogram.[15] Any unintentional discharge of cyanide ions will result in significant environmental risks. The hydrolysis of cyanogenic glycosides in plants such as bitter almonds and bitter cassava as well as cherry, apple, and peach seeds can also create toxic HCN besides industrial disposal. The health effects of excessive exposure to CN⁻ include paralysis of the central nervous system, poisoning of the respiratory enzymes, and hemoglobin poisoning. As a result, breathing becomes difficult, and the body's cells begin to die from hypoxia (low oxygen levels). Therefore, a more sensitive and selective approach for detecting hazardous cyanide anions is still greatly needed.[16]

Various analytical techniques have been applied to determine cyanide ion concentration, including voltammetry, electrochemistry, polarography, and gas chromatography.[17–23]

[a]Department of Chemistry, School of Advanced Sciences, Vellore Institute of Technology, Vellore-632014, India. E-mail: sathiya_kuna@hotmail.com

[b]Institute of Chemical Biology and Nanomedicine, State Key Laboratory of Chemo/Biosensing and Chemometrics, College of Chemistry and Chemical Engineering, Hunan University, Changsha 410082, P. R. China. E-mail: pra3sat@gmail.com

Despite their low detection limits, these techniques need sophisticated sample processing, costly equipment, and trained operators. Due to the increased popularity of fluorescent CN^- sensors, which benefit from excellent selectivity, fast reaction time, and less complex sample preparation, these sensors have advanced significantly in the past several years.[24–37] The reported cyanide fluorescence sensors involved the following mechanistic concepts: coordination, hydrogen bonding interaction, anion-metal affinity, nucleophilic addition reactions, and based on nanotechnology.[32,38–52] Hydrogen bonding, anion metal affinity, and coordination sensors all have significant drawbacks, including a lack of selectivity and interference from competing analytes such as fluoride, phosphate, and acetate ions. However, among the numerous chemosensors described, reaction-based sensors (chemodosimeters) offer the benefits of high specificity, outstanding sensitivity, and rapid response time. Due to the nucleophilic nature of cyanide ions, reaction-based approaches often exhibit high selectivity for cyanide detection. These factors provide the groundwork for the development of reaction-based sensors for the detection of cyanide ions. For example, some of the already reported reaction-based cyanide sensors include imines,[53,54] amide,[55,56] hydrazones,[57] deprotonation mechanism of C–H,[58] acridinium salts,[59] cationic boranes,[60] oxazines.[61] However, slow response time, requirement of high temperature, need of basic medium, high detection limit, less selectivity, inefficiency in aqueous medium hamper the sensing ability of these chemodosimeters. Nucleophilic-based cyanide fluorescence probes have been created and used widely because of their excellent selectivity and increased sensitivity. In recent times, sono-aided chemical precipitation methods have been developed for the synthesis of ZnS, ZnO and quantum dots (QDs).[71,72] It exhibits sensational photocatalytic as well as biological activities.[73,74] Moreover, the biological toxicity levels of ZnS QDs were characterised by UV-visible absorption and fluorescence emission spectrum.[75]

With our interest in CN^- recognition,[34,62,63] in this work, we employ benzothiazole as a fluorophore to develop and manufacture a turn-on cyanide fluorescence probe based on the nucleophilic addition process. A benzothiazole unit was introduced because of its rigid and planar shape and exceptional photophysical characteristics. The donor and acceptor units were covalently bonded together in this hybrid structure by the use of a double bond. Nucleophilic addition to the vinyl double bond causes a disruption of the intramolecular charge transfer (ICT) transition, which results in alterations in both spectral and colour properties. In the probe (**BID**), the benzothiazole moiety functions as an electron donor, while dione acts as an electron receiver, generating fluorescence through Intramolecular Charge Transfer (ICT). Benzothiazole and 1H-indene-1,3(2H)-dione are linked by Knoevenagel condensation reaction, which renders increased conjugation and nucleophilic addition site for recognizing cyanide ions. When CN^- ion was added to an ACN/H_2O solution containing **BID**, the fluorescence spectra indicated that the substantial fluorescence amplification occurred at 512 nm and the solution colour changed to yellow under a 365 nm UV light. At the same time, **BID**'s absorption spectra showed a definite peak at 593 nm with a high intensity.

BID's determined detection limit for CN was 5.97 nM, which is quite low. The fast response to CN^-, strong detecting properties, and ease of setup make this new sensor very promising. The sensor **BID** was used to demonstrate the applicability by detecting CN^- in water, agricultural goods, using test strips, and live cells imaging. It provides a dependable method for detecting CN^- in environmental and biological systems.

Experimental section

Material and apparatus

The required chemicals were obtained from Sigma Aldrich and Alfa Aesar. Chemicals were utilized in the reaction without further purification. Solvents used for synthesis were LR-grade solvents and were used without further purification. Solvents used in spectroscopy were of HPLC grade. Silica gel 100–200 mesh was used for column chromatography. ^1H NMR and ^{13}C NMR spectra were taken in BrukerAscent-400 spectrometer at 25 °C. ^1H NMR and ^{13}C were recorded in $CDCl_3$ and DMSO-d_6. Chemical shifts (δ) are given in ppm relative to TMS internal standard. Absorption spectra were recorded on a Shimadzu 3600 spectrophotometer. Emission spectra were recorded on a PerkinElmer LS-55 luminescence spectrometer. Samples for absorption and emission were taken in a quartz cuvette (4 ml volume).

Synthesis of 2-(3-(benzo[d]thiazol-2-yl)-4-hydroxybenzylidene)-1H-indene-1,3(2H)-dione (BID). The compound 3-(benzo[d] thiazol-2-yl)-4 hydroxybenzaldehyde was dissolved in analytical grade EtOH (15 ml). To this crude solution, indane-1,3-dione (1 mmol) and a catalytic amount of piperidine was added. Then, the reaction mixture was allowed to reflux for about three hours. TLC confirmed the completion of the reaction, and the pure compound had been isolated by column chromatography (in 50% ethyl acetate in n-hexane). The obtained pure **BID** is orange colour solid. The yield was found to be 32%. ^1H NMR (400 MHz, DMSO-d_6): δ 6.968 (s, 1H), 7.425–7.443 (t, 1H, $J = 7.2$ Hz), 7.533–7.552 (t, 1H, $J = 7.6$ Hz), 7.796 (s, 1H), 7.890–7.896 (t, 5H, $J = 2.4$ Hz), 8.068–8.087 (d, 1H, $J = 7.6$ Hz), 8.152–8.171 (d, 1H, $J = 7.6$ Hz), 8.676 (s, 1H), 9.448 (s, 1H). ^{13}C NMR (DMSO-d_6, 100 MHz): δ 100.98, 117.07, 121.49, 125.16, 129.17, 129.42, 131.43, 135.80, 140.89, 152.47, 166.48, 188.14.

Optical selectivity and titration experiments. A stock solution of **BID** (2×10^{-5} M) was prepared in ACN/H_2O (7 : 3) system. A quartz optical cell of a 1 cm optical path was used to record absorption and emission spectra. For each addition of CN^-, the concentration of **BID** was maintained at 2×10^{-5} M. The excitation wavelength used for fluorescence analysis was 320 nm, and we got emissions at 393 nm and 408 nm. Stock solutions of various anions such as F^-, Cl^-, Br^-, I^-, NO_3^-, SCN^-, N_3^-, ClO_4^-, $H_2PO_4^-$, AcO^-, HCO_3^-, SO_4^{2-}, and HSO_4^- were prepared by dissolving their respective salts in double-distilled water.

Results and discussion

Molecular design, synthesis, and structural characterization

With the dione-vinyl group of **BID**, we intended to use the nucleophilic addition reaction of CN^- to develop a sensor

capable of tracking CN^- levels. The β-carbon in the dione-the vinyl group is electron-deficient; thus, CN^- may easily attack this carbon. Due to the presence of two acceptor units on either side of the vinyl group (dione), the **BID** is expected to exhibit increased reactivity and optical response towards CN^-. Scheme 1 depicts the synthesis process and molecular structure of sensor **BID**. The sensor **BID** was successfully synthesized in one step using the Knoevenagel condensation of 3-(benzo[*d*]thiazol-2-yl)-4-hydroxybenzaldehyde with 1*H*-indene-1,3(2*H*)-dione in EtOH in the presence of pyridine to generate **BID** in 32% yield. Compound 3-(benzo[*d*]thiazol-2-yl)-4-hydroxybenzaldehyde was prepared according to a reported procedure. The structural identification of the sensor **BID** was confirmed by ^{1}H NMR, ^{13}C NMR, and HRMS spectra analysis (Fig. S1–S3†).

Solvatochromic properties

BID's UV-vis absorption and photoluminescence properties in increasing polarity solutions have been examined (polarity parameter, Δ*f*, was selected as the solvent polarity metric). As shown in **Fig. S4**,† compound **BID** in toluene solvent exhibits two major absorption peaks at 300 nm and 410 nm, which can be assigned to π–π* electron transfer and intramolecular charge transfer (ICT). The polarity of solvents had only a modest influence on the absorption spectra of **BID** (Fig. 1a) and was essentially unaffected by changes in solvent polarity in ground state energy (excluding DMF and DMSO). Changes in solvent polarity, on the other hand, had a substantial impact on fluorescence spectra (Fig. 1b and Table 1). As the solvent polarity rose, the maximum emission wavelength was redshifted from 610 nm in toluene to 632 nm in CH_3CN, but the relative emission intensity increased simultaneously. The lowest quantum yield (*Φ*) is calculated in the case of toluene, and the highest *Φ* is found in the case of ethanol solvent. The Lippert–Mattaga plot depicts the correlation between the physical characteristics of the solvent (dielectric constant and refractive index) and the Stokes shift of the compound. The graph of Stokes shift of
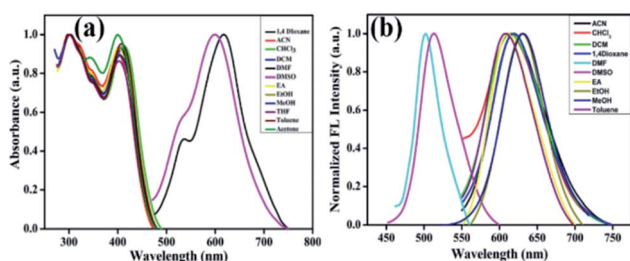

Scheme 1 The synthetic route of sensor BID.

Fig. 1 Normalized absorption (a) and emission spectra (b) of BID in various solvents; excitation wavelength is 398 nm.

Table 1 Photophysical data of BID at room temperature

Solvent	$\lambda_{max}{}^a$ (nm)	$\log E^b$	FWHM^c (nm)	$\lambda_{em}{}^d$ (nm)	$\lambda_s{}^e$ (cm^{-1})	ϕ^f (f)
Toluene	408	4.8	74	610	8116.36	0.0407
Chloroform	413	9.7	60	616	7979.30	0.0598
DCM	408	4.8	90	614	8223.15	0.0554
1,4-Dioxane	405	4.8	80	620	8562.32	0.0504
Ethanol	408	4.8	66	630	8636.78	0.0650
Methanol	404.5	4.7	70	632	8929.6	0.0530
Ethyl acetate	401.5	4.8	72	612	8566.73	0.0471
Acetonitrile	398	4.7	84	618	8818.77	0.0519
DMF	618.5	4.9	40	674	2240.57	0.2574
DMSO	600	4.9	54	682	3079.71	0.3217

^{a} The absorption maximum in nm. ^{b} Molar extinction coefficient in M^{-1} L^{-1} cm^{-1}. ^{c} FWHM in nm. ^{d} The emission maximum in nm. ^{e} The stoke shift in nm. ^{f} Fluorescence quantum yield.

compound **BID** *vs.* orientation polarizability is depicted in Fig. S5.† **BID** showed a rising trend in Stokes shift value with increasing solvent polarity, indicating the presence of ICT and positive solvatochromism. This is a tendency that can only be expected in solvents that do not form hydrogen bonds. However, polar solvents with the capacity to form hydrogen bonds and other particular interactions (complexation and acid–base chemistry) can cause significant alterations. Thus the shift in optical property trend depends on the solvent polarity and can't be entirely predictable.[64]

Sensor BID's optical reaction to the CN- anion

We investigated the optical responsiveness of sensor **BID** in ACN/H_2O (7 : 3, v/v) solution by measuring the changes in absorption and fluorescence emission spectra after adding CN^- anions (2 equiv.). When the representative anions (10 equiv.) F^-, Cl^-, Br^-, I^-, OH^-, AcO^-, $NO_3{}^-$, SCN^-, OCl^-, $HCO_3{}^-$, HS^-, $SO_4{}^{2-}$, $HSO_4{}^-$, $PF_6{}^-$, and $N_3{}^-$ were introduced to the sensor solution, there was almost no change in the solution colour or optical spectra (Fig. 2a). The absorption band, on the other hand, was significantly altered once the solution was added with 2 equiv. of cyanide anion. Two major absorption peaks at 300 nm and 398 nm diminished in their absorbance intensity with the spontaneous appearance of a strong absorbance peak at 593 nm. When the concentration of CN^- ions was increased by 0–2 equiv., the isosbestic spot at 455 nm was found in the UV-vis absorption spectra, as shown in Fig. 2b. The absorbance intensity at 593 nm varied with cyanide concentration and was balanced with the addition of 26 μM CN^-. As shown in Fig. 2c, a strong linear correlation exists between the absorbance intensity at 593 nm and the concentration of cyanide, which ranges from 0 to 24 μM. The linear equation, $y = 0.0097x + 0.0091$, was found from the titration experiment, where y is the absorbance intensity at 593 nm, and x is the concentration of CN^-. The R^2 coefficient of determination is 0.9941, and the error bar is within the reasonable range, indicating that probe **BID** was capable of accurate cyanide detection quantification.
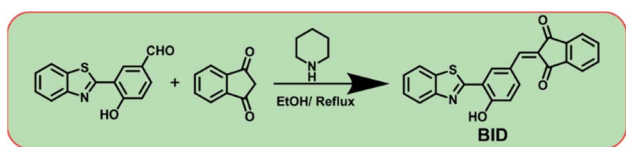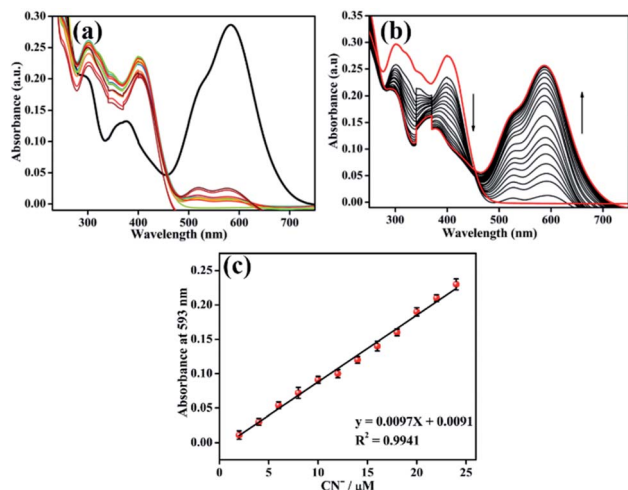
Fig. 2 (a) UV-vis absorption spectrum of sensor **BID** (1×10^{-5} M) in the presence of 10.0 equiv. of different anions in an ACN/H_2O (7 : 3, v/v) solution; (b) sensor **BID** (1×10^{-5} M) absorption spectra in a ACN/H_2O (7 : 3, v/v) solution after addition of different concentrations of CN^- anions (0–2.6 equiv.); (c) linear relationship between A_{593} nm and the cyanide concentration (0–2.6 equiv.).

The fluorescence sensing capability of **BID** towards CN^- in a solution was then investigated. Excitation of probe **BID** at 398 nm resulted in a maximal emission band with low intensity at 625 nm, as illustrated in Fig. 3a. The addition of different anions such as (10 equiv.) F^-, Cl^-, Br^-, I^-, OH^-, AcO^-, NO_3^-, SCN^-, OCl^-, HCO_3^-, HS^-, SO_4^{2-}, HSO_4^-, PF_6^- and N_3^- to the sensor solution did not affect **BID**'s colour and emission spectra remained nearly unchanged. The only significant change occurred when CN^- was introduced, resulting in a blue-shifted fluorescence at 512 nm, was the complete disappearnce of the emission band at 625 nm (Fig. 3a). To further examine **BID**'s CN^- fluorescence sensing characteristics, a series of fluorescence titration studies with CN^- were performed (Fig. 3b). The cyanide ion inhibited the ICT transition inside the molecule,
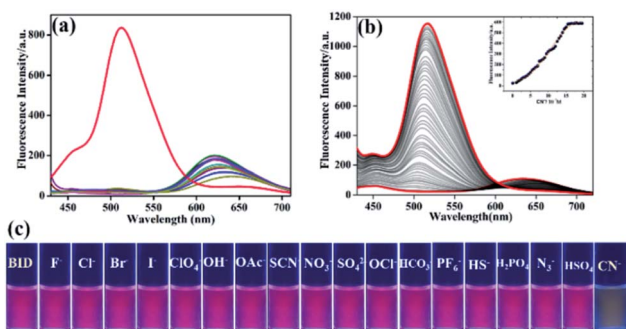
raising the sensor's emission peak at 512 progressively when CN^- ions were gradually added to the sensor solution. Fluorescence increase at 525 nm of **BID** was related to CN^- concentrations throughout an extensive range from 0 to 1.5 μM, as indicated by the correlation coefficient of 0.9947, suggesting that **BID** was an excellent sensor for the quantitative detection of CN^-. This whole event corresponds to a fluorescence colour change of **BID** solution from pink to pale yellow. The sensitivity of **BID** was also investigated fluorometrically. Various solutions of anions were added individually to the **BID** solutions. Meanwhile, the visual colour changes were observed as shown in Fig (3c). The detection limit (LOD) of sensor **BID** for CN^- was determined to be 5.97 nM with a linear range of concentration to be 0–0.5 μM (Fig. S6†), which is far below the allowable content of CN^- in drinking water and the results were compared with previously reported chemosensors for CN^- (Table S3†). The limit of quantitation (LOQ) was estimated to be 1.99 nM, which is calculated based on the equation of $10\sigma/$ slope.

Effect of competitive anions, pH, reaction time and salt concentrations

A competitive experiment was conducted to illustrate the unique selectivity of **BID** for CN^-. Anion CN^- (2.0 equiv.) was applied to sensor **BID** in the presence of other competing analytes (also 2.0 equiv.) evaluated in the optical experiments. Anions coexisting with CN^- did not affect its fluorescence change, as demonstrated in Fig. 4a. These results indicate that sensor **BID** has good selectivity for the fluorescence detection of cyanide anion in the presence of another competing anion, making it particularly relevant in practical applications for cyanide detection. In addition, the impact of pH on cyanide anion sensing was investigated. Fig. 4b depicts the changes in
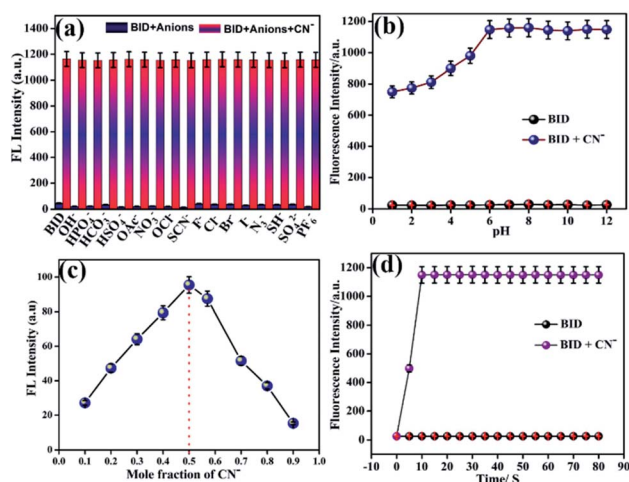

Fig. 3 (a) Fluorescence spectra of **BID** (1×10^{-6} M) in the presence of different analytes (10.0 equiv. 1×10^{-6} M); (b) fluorescence emission of probe **BID** (1×10^{-6} M) in ACN/H_2O (7 : 3, v/v) solution in the presence of a varying concentration of CN^- from 0 to 1.5 μM, inset shows the plot of I_{525} vs. the concentration of CN^-; (c) changes in the solution fluorescence color of **BID** with different analytes under a UV light of 365 nm.

Fig. 4 (a) Competitive experiments of the **BID** + CN^- system with interfering anions (λ_{ex} = 398 nm) in ACN/H_2O (7 : 3); (b) the fluorescence intensity of **BID** (1 μM) in the absence and presence of CN^- (λ_{ex} = 398 nm) as a function of pH (1.0–12.0); (c) Job's plot for determining the stoichiometry of **BID** and CN^- ions; (d) the time-dependent fluorescence spectrum of **BID** toward CN^- in ACN/H_2O (7 : 3).

sensor **BID**'s fluorescence at 525 nm as a function of pH, with and without the addition of CN⁻. It was found that the fluorescence signal of the free sensor **BID** in the pH range of 1.0 to 12.0 was very weak and was only marginally influenced by H⁺ or OH⁻. When CN⁻ is present in the pH range of 1.0–12.0, the fluorescence at 525 nm of the sensor **BID** increases considerably up to pH = 6, and the **BID** fluorescence response to CN⁻ between 6.0 and 12.0 was almost pH-independent. Because CN⁻ anions are quickly converted to weak acid, HCN and due to the protonation of **BID** (the guest), the host-guest contact is reduced, and the fluorescence emission of **BID** is reduced or diminished. The binding mode of **BID**–CN⁻ was examined by Job's plot experiments. Thereby, the complex (**BID**–CN⁻) demonstrates a maximum absorbance in the 0.5 mole fraction. Hence, 1 : 1 stoichiometry of complexation has been achieved (Fig. 1c). To determine the probe **BID**'s capability for fast cyanide detection, we studied the time courses of the fluorescence intensity increase of probe **BID** (1×10^{-6} M) in the presence of CN⁻ (2 equiv.) in a mixture of ACN/H₂O (7 : 3, v/v) at room temperature (Fig. 4d). Fig. S7† illustrates the fluorescence changes in **BID** and **BID**–CN⁻ at various salt concentrations demonstrate that the changes in the exhibited fluorescence curve are minor in NaCl solution, showing that the synthesised **BID** and **BID**–CN⁻ are highly stable.

Investigation of sensing mechanism

Further, we decided to investigate the **BID**–CN⁻ reaction product to learn more about the sensing mechanism of sensor **BID** for CN⁻ exposure. The ¹H NMR spectra data in DMSO-d_6 at room temperature before and after cyanide anion addition are shown in Fig. 5a. A peak at 8.75 ppm corresponds to the vinyl proton (Ha), which was eliminated following the addition of 1.0 equiv. CN⁻, whereas a new signal at 5.18 ppm corresponds to the α-proton H_b appeared. Additionally, the phenolic proton, which appeared at 9.44 ppm, presented an up-field shift to 8.48 ppm. Meanwhile, the aromatic proton signals from 1*H*-indene-1,3(2*H*)-dione exhibited a significant up-field shift compared to those from the **BID**. These outcomes may be
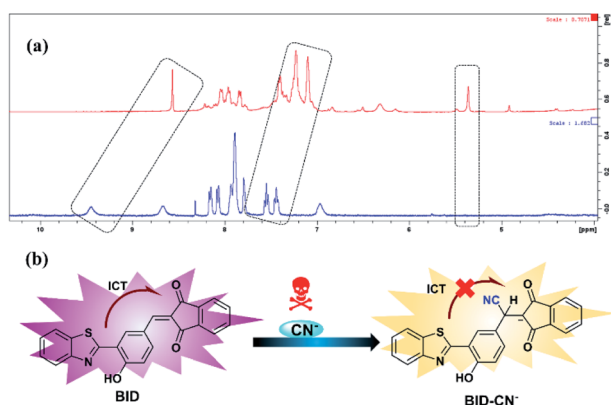
explained by **BID**'s nucleophilic addition to CN⁻, which disrupts conjugation between the benzothiazole framework and the 1*H*-indene-1,3(2*H*)-dione group and decreases dione's electron-withdrawing capacity. Furthermore, HRMS analysis verified the formation of the newly created adduct (**BID**–CN⁻) (Fig. S3†). According to mass spectral analysis, the peak of **BID** was found to be 383.0618 *m/z*. After the one equiv. of CN⁻ was added into the **BID** solution, the **BID**–CN⁻ peak with a mass of 408.0566 *m/z* appeared, showing conclusively that **BID** : CN⁻ is a 1 : 1 stoichiometric ratio. FT-IR spectra were also used to validate the mechanism of interaction between **BID** and CN⁻. As depicted in Fig. S8,† it was noticed that in the presence of CN⁻ (1.0 equiv.), the typical stretching bands for the saturated hydrocarbon (CH) group emerged at 2972 and 2858 cm⁻¹, while the distinctive stretching vibration of (C=C) at 1581 cm⁻¹ entirely vanished. Meanwhile, the absorption peak of keto (C=O) group stretching vibrations was moved from 1683 to 1726 cm⁻¹.

Theoretical calculations

The complex formation between the CN⁻ ion and **BID** was studied further at the molecular level utilizing a density functional theory-based computational method. The density functional theory at the B3LYP/631 G(d) level was utilized effectively to predict photochromism and reaction-based photochromic molecules with high accuracy.[29,64–70] The entire geometry optimizations of the probe **BID** and its interaction with CN⁻ were performed using the aforementioned technique, and its structure is shown in Fig. S9.† The transition energies and relative oscillator strengths of the probable important transitions for the **BID** and **BID** + CN⁻, have been found (Table S1†). As shown in Fig. 6, HOMO of **BID** has electron densities that are restricted to the 1*H*-indene-1,3(2*H*)-dione group alone, and it has been calculated that there is 3.43 eV of energy difference (ΔE) between the HOMO and LUMO ($E_{HOMO} = -6.4120$ eV and $E_{LUMO} = -2.9777$ eV). As a result of the ICT that happens in the

Fig. 5 (a) ¹H NMR spectra (400 Hz, DMSO-d_6) of sensor **BID** in the absence and presence of CN⁻ (1.0 equiv.). (b) The suggested response mechanism for the sensor **BID** in conjunction with CN⁻.
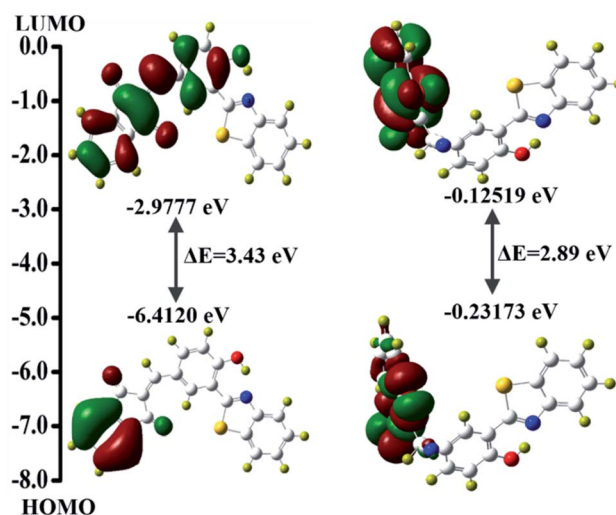

Fig. 6 The optimal structures of **BID** and **BID** + CN⁻ determined by DFT/B3LYP methods.

excited state, it is discovered that a considerable amount of electron transfer occurs between the benzothiazole unit and the 1H-indene-1,3(2H)-dione functionality (LUMO). Despite this, when the electron allocation in **BID** + CN^- is taken into consideration, both the HOMO and LUMO localized entirely inside the 1H-indene-1,3(2H)-dione functionality, resulting in the electronic excitation occurring in the same chromophore, which severely limits the ICT effect.

BID loaded paper-based indicators for CN^- ion

To further evaluate the chemosensor's utility as a quick approach for detecting CN^- levels in water samples, paper test strips were impregnated with the chemosensor **BID** (2×10^{-3} M) using a concentrated acetonitrile solution. After dropping different anion solutions (2 mM) onto a "fluorescence paper-based indicator," the colour change was observed while exposed to a 365 nm UV light. Fig. 7 exhibited that the paper-based fluorescent indicator loaded with **BID** presented dark pink emission. The fluorescence emission remained constant even after adding various anions as tested in the selectivity study. As expected, it could be observed that the fluorescence was blue after CN^- was dropped. As predicted, it was apparent that the fluorescence had changed from pink to blue once the CN^- was dropped. **BID** paper-based indicator can thus be used for the visual inspection of CN^- in an easy and straightforward manner.

Application in real samples analysis

As a result of worldwide industrial operations and improper waste disposal, many water sources have become severely polluted, endangering aquatic life and the ecosystem. Thus, the development of an effective analytical technique for quantifying CN^- in environmental samples is imperative. The sensitivity of the **BID** to the detection of CN^- in real water samples such as tap water, distilled water, and pond water from Vellore Institute of Technology (VIT), Vellore campus, was assessed using the conventional addition approach. The collected water samples were filtered three times with a 0.45 mm membrane filter, then spiked with a particular amount of CN^-, diluted ten times, and were put to the test using standard procedures (Table 2).

The standard addition technique was used to calculate the CN^- concentration, which involved the addition of 2, 4, and 6 μM of CN^- to the above-mentioned water samples. It can be seen from Table 1 that, with satisfactory recovery (97.4–100.2%) and low RSD (0.024–1.37%), the **BID** sensor was able to detect the spiked CN^-, demonstrating the feasibility and reliability of the sensor **BID** for the determination of CN^- in a variety of

Table 2 Results of CN^- readings in water samples from the environment

Sample	Spiked (μM)	Found ($X^a \pm SD^b$) (μM)	Recovery (%)	RSD^c (%)
Tap water	2.0	1.992 ± 0.007	99.6	0.18
	4.0	3.998 ± 0.007	99.9	0.22
	6.0	6.009 ± 0.003	100.2	0.36
Distilled water	2.0	2.003 ± 0.002	100.2	0.34
	4.0	3.992 ± 0.007	99.8	0.44
	6.0	6.011 ± 0.008	100.2	0.62
Pond water	2.0	1.948 ± 0.004	97.4	0.60
	4.0	3.921 ± 0.006	98.0	0.51
	6.0	5.933 ± 0.005	98.9	0.78

^{a} Mean of three determinations. ^{b} SD: standard deviation. ^{c} RSD: relative standard deviation.

environmental water samples. In addition, the obtained results were cross verified with ^{1}H-NMR based analysis. In this method, peak intensity gradually increases at 5.18 ppm and is used to derive ^{1}H-NMR calibration plot (Fig S10 and Table S2†).

Bio-imaging application

Additionally, *Escherichia coli* (*E. coli*) cells were employed as a model system for further use of as-synthesized **BID** on bacterium imaging. As a result, preliminary cytotoxicity testing was performed. As shown in Fig. S11,† there was no discernible reduction in *E. coli* viability when **BID** concentrations were increased to 20 μM, supporting **BID's** extremely minimal impact on *E. coli*. Additionally, it was discovered that *E. coli* had a distinct fluorescent red short dot form and that no apparent restriction of *E. coli* growth was seen under the fluorescence microscope. In the other group, **BID** was incubated with *E. coli*
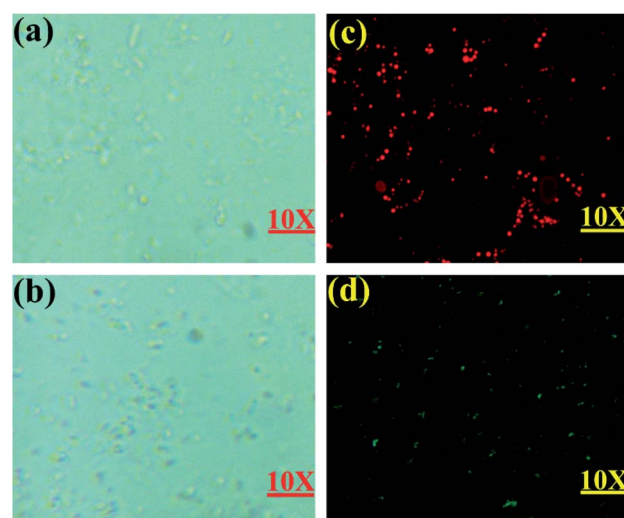

Fig. 8 Fluorescent cell imaging: (a) and (b) bright-field image of *E. coli* cells using the green filter of 510 to 560 nm; (c) fluorescent field image of **BID** treated *E. coli* cells; (d) fluorescent field image of **BID** treated *E. coli* cells incubated with CN^- ions using the yellow filter of 532 to 587 nm.

Fig. 7 Photographs of **BID** in the presence of various anions and CN^- under a UV lamp at 365 nm.

bacteria for 20 minutes at 37 °C before being incubated with 20 μM of CN^- for another 20 minutes, resulting in the development of green fluorescence (Fig. 8d). The results showed that the probe was capable of detecting the CN^- ion in live cells.

Conclusions

In summary, a new fluorescence sensor **BID** based on benzothiazole and a 1*H*-indene-1,3(2*H*)-dione derivative for detecting CN^- has been developed. Optical studies revealed that **BID** has excellent sensitivity and selectivity toward CN^- while other anions examined have no effect. Under UV light, a dramatic fluorescent color shift from pink to pale yellow was noticed, as well, as a substantial fluorescence increase was observed when CN^- was added to the sensor **BID** solution. The sensing mechanism was built on the nucleophilic addition reaction of the sensor with CN^-. This was also verified by optical studies, ^{1}H NMR titration, FT-IR spectra, HRMS, and DFT/TD-DFT calculations. The detection limit was determined to be as low as 5.97 nM, and the quick reaction time following the addition of CN^-, indicates that sensor **BID** may be utilized as an effective sensor for CN^- detection. Additionally, the sensor **BID** was successfully utilized to detect CN^- in environmental water samples, enabling the sensor's expansion into food industries. Furthermore, the sensor **BID** responds to CN^- with fluorescence, allowing image detection and real-time monitoring of CN^- in live *E. coli* cells.

Conflicts of interest

There are no conflicts to declare.

Acknowledgements

Notes and references

1 R. V. Rathod, S. Bera and D. Mondal, *Spectrochim. Acta, Part A*, 2020, **238**, 118419.

2 A. Sala, H. Brisset, A. Margaillan, J.-U. Mullot and C. Branger, *TrAC, Trends Anal. Chem.*, 2022, **148**, 116536.

3 M. Qiao, L. Ding and F. Lv, *Coord. Chem. Rev.*, 2021, **432**, 213696.

4 H. Gomaa, S. El-Safty, M. A. Shenashen, S. Kawada, H. Yamaguchi, M. Abdelmottaleb and M. F. Cheira, *ACS Sustainable Chem. Eng.*, 2018, **6**, 13813–13825.

5 I. M. El-Sewify, M. A. Shenashen, A. Shahat, H. Yamaguchi, M. M. Selim, M. M. H. Khalil and S. A. El-Safty, *J. Lumin.*, 2018, **198**, 438–448.

6 I. M. El-Sewify, M. A. Shenashen, A. Shahat, M. M. Selim, M. M. H. Khalil and S. A. El-Safty, *Microchem. J.*, 2018, **139**, 24–33.

7 S. A. El-Safty, M. Khairy, M. A. Shenashen, E. Elshehy, W. Warkocki and M. Sakai, *Nano Res.*, 2015, **8**, 3150–3163.

8 S. A. El-Safty and M. A. Shenashen, *Sens. Actuators, B*, 2013, **183**, 58–70.

9 M. Khairy, S. A. El-Safty, M. A. Shenashen and E. A. Elshehy, *Nanoscale*, 2013, **5**, 7920–7927.

10 V. Amendola and L. Fabbrizzi, *Chem. Commun.*, 2009, 513–531.

11 S. Liu, D. Yang, Y. Liu, H. Pan, H. Chen, X. Qu and H. Li, *Sens. Actuators, B*, 2019, **299**, 126937.

12 R. M. Duke, E. B. Veale, F. M. Pfeffer, P. E. Kruger and T. Gunnlaugsson, *Chem. Soc. Rev.*, 2010, **39**, 3936–3953.

13 P. A. Gale, J. T. Davis and R. Quesada, *Chem. Soc. Rev.*, 2017, **46**, 2497–2519.

14 J. T. Davis, P. A. Gale and R. Quesada, *Chem. Soc. Rev.*, 2020, **49**, 6056–6086.

15 L. Xue, R. Wang, S. Qi, H. Xu, X. Wang, L. Wu, Q. Yang, J. Du and Y. Li, *Talanta*, 2021, **225**, 122100.

16 A. Ishii, H. Seno, and K. Watanabe-Suzuki, O. Suzuki and T. Kumazawa, *Determination of Cyanide in Whole Blood by Capillary Gas Chromatography with Cryogenic Oven Trapping*, https://pubs.acs.org/doi/pdf/10.1021/ac980498b, accessed 29 August, 2021.

17 E. PRandviir and C. E. Banks, *TrAC, Trends Anal. Chem.*, 2015, **64**, 75–85.

18 B. L. Mitchell, G. A. Rockwood and B. A. Logue, *J. Chromatogr. B*, 2013, **934**, 60–65.

19 H.-I. Kang and H.-S. Shin, *Anal. Chem.*, 2015, **87**, 975–981.

20 T. Suzuki, A. Hioki and M. Kurahashi, *Anal. Chim. Acta*, 2003, **476**, 159–165.

21 S. Dadfarnia, A. M. Haji Shabani, F. Tamadon and M. Rezaei, *Microchim. Acta*, 2007, **158**, 159–163.

22 M. Shamsipur and H. R. Rajabi, *Mater. Sci. Eng., C*, 2014, **36**, 139–145.

23 H. R. Rajabi, M. Shamsipur, A. A. Khosravi, O. Khani and M. H. Yousefi, *Spectrochim. Acta, Part A*, 2013, **107**, 256–262.

24 Q. Zou, F. Tao, Z. Xu, Y. Ding, Y. Tian and Y. Cui, *Anal. Methods*, 2019, **11**, 5553–5561.

25 M. Kargar, H. R. Darabi, A. Sharifi and A. Mostashari, *Analyst*, 2020, **145**, 2319–2330.

26 W.-Z. Zhang, Z.-Z. Chen, X.-J. Han and W.-K. Dong, *Spectrochim. Acta, Part A*, 2021, **258**, 119815.

27 Z. Shi, Y. Tu, R. Wang, G. Liu and S. Pu, *Dyes Pigm.*, 2018, **149**, 764–773.

28 R. Chandra, A. Ghorai and G. K. Patra, *Sens. Actuators, B*, 2018, **255**, 701–711.

29 Q. Niu, L. Lan, T. Li, Z. Guo, T. Jiang, Z. Zhao, Z. Feng and J. Xi, *Sens. Actuators, B*, 2018, **276**, 13–22.

30 S. Bhardwaj, N. Maurya and A. K. Singh, *Sens. Actuators, B*, 2018, **260**, 753–762.

31 K. Deng, L. Wang, Q. Xia, R. Liu and J. Qu, *Sens. Actuators, B*, 2019, **296**, 126645.

32 C. Yin, F. Huo, M. Xu, C. L. Barnes and T. E. Glass, *Sens. Actuators, B*, 2017, **252**, 592–599.

33 P. Ravichandiran, A. Boguszewska-Czubara, M. Masłyk, A. P. Bella, P. M. Johnson, S. A. Subramaniyan, K. S. Shim and D. J. Yoo, *Dyes Pigm.*, 2020, **172**, 107828.

34 S. Munusamy, S. Swaminathan, D. Jothi, V. P. Muralidharan and S. K. Iyer, *RSC Adv.*, 2021, **11**, 15656–15662.

35 A. K. Mahapatra, K. Maiti, S. K. Manna, R. Maji, C. D. Mukhopadhyay, B. Pakhira and S. Sarkar, *Chem.– Asian J.*, 2014, **9**, 3623–3632.

36 P. Torawane, S. K. Sahoo, A. Borse and A. Kuwar, *Luminescence*, 2017, **32**, 1426–1430.

37 C.-B. Bai, J. Zhang, R. Qiao, Q.-Y. Zhang, M.-Y. Mei, M.-Y. Chen, B. Wei, C. Wang and C.-Q. Qu, *Ind. Eng. Chem. Res.*, 2020, **59**, 8125–8135.

38 K. Wang, X. Yu, Y. Zhu, M. Xing, M. Liang, Y. Sun, D. Cao, R. Guan and Z. Liu, *J. Mol. Struct.*, 2018, **1173**, 647–652.

39 W.-J. Qu, H.-H. Yang, J.-P. Hu, P. Qin, X.-X. Zhao, Q. Lin, H. Yao, Y.-M. Zhang and T.-B. Wei, *Dyes Pigm.*, 2021, **186**, 108949.

40 K.-S. Lee, J. T. Lee, J.-I. Hong and H.-J. Kim, *Chem. Lett.*, 2007, **36**, 816–817.

41 T.-B. Wei, J.-D. Ding, J.-F. Chen, B.-B. Han, X.-M. Jiang, H. Yao, Y.-M. Zhang and Q. Lin, *New J. Chem.*, 2018, **42**, 1271–1275.

42 P. R. Lakshmi, P. S. Kumar and K. P. Elango, *Spectrochim. Acta, Part A*, 2020, **229**, 117974.

43 L. Wang, Z.-L. Wei, Z.-Z. Chen, C. Liu, W.-K. Dong and Y.-J. Ding, *Microchem. J.*, 2020, **155**, 104801.

44 P. S. Kumar, S. Ciattini, C. Laura and K. P. Elango, *J. Mol. Liq.*, 2020, **317**, 113970.

45 S. Ramesh and S. Kumaresan, *Microchem. J.*, 2021, **169**, 106584.

46 Q. Wu, S. Wang, E. Hao and L. Jiao, *Spectrochim. Acta, Part A*, 2021, **247**, 119102.

47 Y. Wang, J. Wang and Q. Xian, *Talanta*, 2018, **190**, 487–491.

48 L. Patra, K. Aich, S. Gharami and T. K. Mondal, *J. Lumin.*, 2018, **201**, 419–426.

49 G. Kumar, N. Gupta, K. Paul and V. Luxami, *Sens. Actuators, B*, 2018, **267**, 549–558.

50 S. Li, F. Huo, K. Ma, Y. Zhang and C. Yin, *New J. Chem.*, 2021, **45**, 1216–1220.

51 B. Aydıner, Ö. Şahin, D. Çakmaz, G. Kaplan, K. Kaya, Ü. Ö. Özdemir, N. Seferoğlu and Z. Seferoğlu, *New J. Chem.*, 2020, **44**, 19155–19165.

52 H. Gomaa, M. A. Shenashen, A. Elbaz, S. Kawada, T. A. Seaf El-Nasr, M. F. Cheira, A. I. Eid and S. A. El-Safty, *J. Colloid Interface Sci.*, 2021, **604**, 61–79.

53 B. Yilmaz, M. Keskinates, Z. Aydin and M. Bayrakci, *J. Photochem. Photobiol., A*, 2022, **424**, 113651.

54 A. Pundi, J. Chen, C.-J. Chang, S.-R. Hsieh, M.-C. Lee, C.-H. Chou and T.-D. Way, *Spectrochim. Acta, Part A*, 2021, **262**, 120139.

55 E. Kandemir, M. Özkütük, B. Aydıner, N. Seferoğlu, H. Erer and Z. Seferoğlu, *J. Mol. Struct.*, 2022, **1249**, 131593.

56 T. P. Martyanov, A. A. Kudrevatykh, E. N. Ushakov, D. V. Korchagin, I. V. Sulimenkov, S. G. Vasil'ev, S. P. Gromov and L. S. Klimenko, *Tetrahedron*, 2021, **93**, 132312.

57 X. Lv, J. Liu, Y. Liu, Y. Zhao, M. Chen, P. Wang and W. Guo, *Org. Biomol. Chem.*, 2011, **9**, 4954–4958.

58 T. Zhu, Z. Li, C. Fu, L. Chen, X. Chen, C. Gao, S. Zhang and C. Liu, *Tetrahedron*, 2020, **76**, 131479.

59 Y.-K. Yang and J. Tae, *Org. Lett.*, 2006, **8**, 5721–5723.

60 T. W. Hudnall and F. P. Gabbaï, *J. Am. Chem. Soc.*, 2007, **129**, 11978–11986.

61 S. Sanjabi, J. Keyvan Rad and A. R. Mahdavian, *J. Photochem. Photobiol., A*, 2022, **424**, 113626.

62 D. Jothi, S. Munusamy and S. K. Iyer, *J. Photochem. Photobiol., A*, 2021, **420**, 113491.

63 D. Jothi, S. Munusamy, S. Sawminathan and S. K. Iyer, *RSC Adv.*, 2021, **11**, 11338–11346.

64 S. Nigam and S. Rutan, *Appl. Spectrosc.*, 2001, **55**, 362A–370A.

65 S. Sawminathan, S. Munusamy, D. Jothi and S. K. Iyer, *ChemistrySelect*, 2021, **6**, 858–864.

66 Q. Zou, F. Tao, H. Wu, W. W. Yu, T. Li and Y. Cui, *Dyes Pigm.*, 2019, **164**, 165–173.

67 T. Sheshashena Reddy, H. Moon and M.-S. Choi, *Spectrochim. Acta, Part A*, 2021, **252**, 119535.

68 H. Jain, N. Deswal, A. Joshi, C. N. Ramachandran and R. Kumar, *Anal. Methods*, 2019, **11**, 3230–3243.

69 P. Ghorai, K. Pal, P. Karmakar and A. Saha, *Dalton Trans.*, 2020, **49**, 4758–4773.

70 G. Shally, V. Kumar, I. Althagafi, A. Kumar, D. Singhal, A. Kumar, R. Gupta and R. Pratap, *New J. Chem.*, 2020, **44**, 15559–15566.

71 H. R. Rajabi, F. Karimi, H. Kazemdehdashti and L. Kavoshi, *J. Photochem. Photobiol., B*, 2018, **181**, 98–105.

72 H. R. Rajabi, R. Naghiha, M. Kheirizadeh, H. Sadatfaraji, A. Mirzaei and Z. M. Alvand, *Mater. Sci. Eng., C*, 2017, **78**, 1109–1118.

73 F. Karimi, H. R. Rajabi and L. Kavoshi, *Ultrason. Sonochem.*, 2019, **57**, 139–146.

74 H. R. Rajabi, H. Arjmand, H. Kazemdehdashti and M. Farsi, *J. Environ. Chem. Eng.*, 2016, **4**, 2830–2840.

75 B. Hemmateenejad, M. Shamsipur, F. Samari and H. R. Rajabi, *J. Iran. Chem. Soc.*, 2015, **12**, 1729–1738.